# The ACS Survey of Galactic Globular Clusters. I.<sup>1</sup> Overview and Clusters Without Previous *HST* Photometry

Ata Sarajedini

Department of Astronomy, University of Florida, 211 Bryant Space Science Center, Gainesville, FL 32611

ata@astro.ufl.edu

Luigi R. Bedin

European Southern Observatory, Garching, Karl-Schwarzschild-Str. 2, D-85748, D, EU

lbedin@eso.org

Brian Chaboyer and Aaron Dotter

Department of Physics and Astronomy, Dartmouth College, 6127 Wilder Laboratory, Hanover, NH 03755

chaboyer@heather.dartmouth.edu, Aaron.L.Dotter@dartmouth.edu

Michael Siegel

University of Texas, McDonal Observatory, 1 University Station, C1402, Austin TX, 78712 siegel@astro.as.utexas.edu

Jay Anderson

Department of Physics and Astronomy, Rice University MS-108, Houston, TX 77005
jay@eeyore.rice.edu

Antonio Aparicio

University of La Laguna and Instituto de Astrofísica de Canarias La Laguna, Canary Islands, Spain

antapaj@iac.es

Ivan King

Dept. of Astronomy, Univ. of Washington, Box 351580, Seattle, WA 98195-1580 king@astro.washington.edu

## Steven Majewski

Dept. of Astronomy, University of Virginia, P.O. Box 400325, Charlottesville, VA 22904-4325

# srm4n@virginia.edu

#### A. Marín-Franch

Department of Astronomy, University of Florida, 211 Bryant Space Science Center, Gainesville, FL 32611

amarin@astro.ufl.edu

Giampaolo Piotto

Dipartimento di Astronomia, Università di Padova, 35122 Padova, Italy piotto@pd.astro.it

I. Neill Reid

Space Telescope Science Institute, 3700 San Martin Drive, Baltimore MD 21218
inr@stsci.edu

Alfred Rosenberg

Instituto de Astrofísica de Canarias, Vía Láctea s/n, E-38200 La Laguna, Spain

alf@iac.es

#### ABSTRACT

We present the first results of a large ACS Survey of Galactic globular clusters. This Hubble Space Telescope (HST) Treasury project is designed to obtain photometry with S/N  $\gtrsim 10$  for main sequence stars with masses  $\gtrsim 0.2 M_{\odot}$  in a sample of globulars using the Advanced Camera for Surveys (ACS) Wide Field Channel. Here we focus on clusters without previous HST imaging data. These include NGC 5466, 6779, 5053, 6144, Palomar 2, E 3, Lyngå 7, Palomar 1, and NGC 6366. Our CMDs extend reliably from the horizontal branch to as much as seven magnitudes fainter than the main sequence turnoff and represent the deepest CMDs published to-date for these clusters. Using fiducial sequences for

three standard clusters (M92, NGC 6752, and 47 Tuc) with well-known metallicities and distances, we perform main sequence fitting on the target clusters in order to obtain estimates of their distances and reddenings. These comparisons along with fitting the cluster main sequences to theoretical isochrones yield ages for the target clusters. We find that the majority of the clusters have ages that are consistent with the standard clusters at their metallicities. The exceptions are E 3 which appears  $\sim$ 2 Gyr younger than 47 Tuc, and Pal 1, which could be as much as 8 Gyr younger than 47 Tuc.

Subject headings: globular clusters: individual (E 3, Lynga 7, NGC 5053, NGC 5466, NGC 6144, NGC 6366, NGC 6779, Palomar 1, Palomar 2) — Hertzsprung-Russell diagram

## 1. Introduction

We present the first results of a 134-orbit Hubble Space Telescope (HST) Treasury program to conduct an ACS Survey of Galactic Globular Clusters (GC). This project is designed to obtain uniform photometry with S/N  $\gtrsim 10$  for stars as faint as  $0.2\mathcal{M}_{\odot}$  ( $M_V \lesssim 10.7$ ) along the main sequence for approximately half of the nearest known Milky Way GCs using the Wide Field Channel (WFC) of the Advanced Camera for Surveys (ACS). The survey will produce an image atlas and source catalog with astrometry and photometry for stars in the target clusters using both newly obtained ACS observations as well as archival ACS and Wide Field Planetary Camera 2 imaging, where available. In the spirit of the HST Treasury concept, the overall goal of this "legacy" survey is to investigate fundamental aspects of Galactic GCs (e.g., luminosity functions, reddenings, distances, ages, proper motions, binary fractions, to name a few) and provide a lasting contribution to cluster studies by creating a uniquely deep and uniform database of a large sample of Galactic GCs.

Our target list includes 66 GCs chosen by a number of criteria, the most important of which are proximity to the Sun  $((m-M)_0 \le 16.5)$  and low-reddening  $(E(B-V) \le 0.35)$ . However, we have also included a few clusters of intrinsic interest such as those believed to be associated with the Sagittarius dwarf spheroidal galaxy and a number of clusters in

<sup>&</sup>lt;sup>1</sup>Based on observations with the NASA/ESA *Hubble Space Telescope*, obtained at the Space Telescope Science Institute, which is operated by AURA, Inc., under NASA contract NAS 5-26555, under programs GO-10775 (PI: Sarajedini).

the direction of the Galactic bulge. The full details of our target list will be published in a forthcoming paper.

This first paper in our survey is concerned with GCs in our target list that have not been previously imaged by HST. These include the metal-poor clusters NGC 5466, 6779 (M56), 5053, and 6144, the intermediate metallicity cluster Palomar 2, and the metal-rich clusters E 3, Lyngå 7, Palomar 1, and NGC 6366. The clusters are ordered, here as elsewhere in this paper, by metallicity. In the next section, we summarize the observations and data reduction, which are generally similar for all clusters in our program. The resultant color-magnitude diagrams are presented and discussed in Sec. 3. Main sequence fits and comparisons with theoretical isochrones are included in Sec. 4 and 5, respectively. Section 6 presents a summary of our results.

#### 2. Observations and Data Reduction

The observations of our program clusters were obtained with the HST/ACS/WFC instrument in the F606W ( $\sim V$ ) and F814W ( $\sim I$ ) filters. Each cluster was centered in the ACS field and observed for two orbits, one orbit for each filter, with one short exposure per filter (except for Pal 2) and four to five long exposure frames. The long exposures were dithered to fill in the gap between the two CCDs of ACS. Table 1 presents the log of the observations.

The process of deriving photometry from the short and long exposures and combining the results will be fully described in an upcoming paper (Anderson et al. 2007, in preparation). To summarize, we reduced each \_FLT exposure independently using the program img2xym\_WFC.09x10, which is documented in Anderson & King (2006). The program uses an array of 9×10 PSFs to treat the spatial variability of the WFC PSF. The routine also allows for a spatially constant perturbation adjustment for the PSF to better match each individual exposure. (The perturbation adjustment for the PSF was possible only on exposures that had a sufficient number of well-exposed stars; this ruled out all of the short exposures.)

The above computer program went through each image pixel by pixel and used the PSF model to get a flux and a position for every source that had no brighter neighbors within 3 pixels and had at least 50 e<sup>-</sup>'s above sky in a 3×3-pixel aperture. We correct the source's position for distortion using the prescription in Anderson (2006) and find the transformation from each frame into a single reference frame centered on the cluster core.

We then collate the deep star lists in the reference frame, identifying a star wherever there are three or more coincident detections in the deep exposures for each filter. This collation procedure naturally removes any cosmic rays or warm pixels that may have strayed into the deep lists for the individual exposures. We now have one star list for each of the two filters. This list contains only stars that are below the saturation limit in the deep exposures. Since each star in this list has been observed in a minimum of three exposures independently, we also have an estimate of the error in its photometry from the rms magnitude about the mean of the independent observations.

We supplement this list with the star lists for the short exposures. We first find an empirical photometric-zeropoint offset between the short and deep exposures and add to the deep list for each filter any star in the short exposures that is within 0.75 magnitudes of saturation or brighter in the deep list. Stars that are saturated in the short exposures are measured by fitting the PSF to their unsaturated pixels and are included in the list, even though their photometry and astrometry are less accurate. Thus, in the end, we have a list of stars found in each of the two filters. Our final star catalog is produced by merging the F606W and F814W lists, keeping only stars found in both filters. It is important to emphasize at this point that this 'first pass' photometry includes only the uncrowded stars (i.e. those with no brighter neighbors within 3 pixels). The 'final pass' reduction, where we relax this crowding restriction, will include many more stars and will therefore be more complete. The photometric catalog that the Treasury project makes available to the community will include only the final pass data.

The resultant instrumental magnitudes must be corrected for the effects of charge transfer efficiency (CTE) before being transformed to a standard system. To facilitate this, we rely upon the formalism of Reiss & Mack (2004, hereafter RM2004). We begin by noting that all of our long exposure observations, except for those of E3, exhibit background sky values greater than ~30 electrons. Equation 2 of RM2004 suggests that, at these sky levels, the CTE correction is less than ~0.005 mag for all stellar magnitudes and y-coordinates. Even in the case of E3 where the mean sky level is ~10 electrons, Fig. 2 of RM2004 shows that the CTE correction is typically 0.01 mag. Based on this, we choose not to correct the long exposure photometry for the CTE effect and proceed to correct the short exposure photometry using Equation 2 of RM2004. These corrections are relatively small amounting to ~0.03 mag for the faintest stars on the short exposure frames roughly equalling the expected random errors for these stars. To check the efficacy of these corrections, we examine the difference in magnitude of a given star between the long and short exposures as a function of Y-position to be sure that there is no trend present. Since the corrections are approximately the same on the F606W and F814W filters, the colors are minimally affected.

We calibrate the photometry to the ACS/WFC VEGAmag system following the procedure given in Bedin et al. (2005) using the most updated encircled energy distributions

and the official zeropoints given by Sirianni et al. (2005). The result of this procedure is photometry that reliably extends from the horizontal branch (HB) to several magnitudes below the main sequence turnoff (MSTO). <sup>2</sup>

## 3. Color-Magnitude Diagrams

The CMDs derived from our HST/ACS observations of the target clusters are shown in Figs. 1 through 9. In each case, the crosses indicate stars affected by at least one saturated pixel in either or both of the F606W and F814W short exposure images. All four of the metal-poor clusters display predominantly blue HBs along with significant blue straggler sequences. Six of the nine clusters also show rich populations of unresolved main sequence binaries as evidenced by the parallel sequences located as much as 0.75 mag brighter than the MS. This is not particularly surprising given that we are imaging the central regions of these clusters where mass segregation has enhanced the binary populations. We should also note that some of these CMDs may contain significant white dwarf sequences. Confirmation of these sequences will require star/galaxy image classification, which will be presented in a future paper.

To fully appreciate the properties of these CMDs, it is important to examine them within the context of existing ground-based photometry of these clusters.

NGC 5466: The most recent CMDs of this cluster have been presented by Jeon et al. (2004), Rosenberg et al. (2000b), and Corwin, Carney, & Nifong (1999). Because of its substantial population of blue stragglers, the majority of prior CMD studies have focused on these stars and their photometric variability. This cluster is of exceptionally low stellar density even near its center; it is probably because of this that NGC 5466 has not been a primary target of HST studies. However, it is clear from Fig. 1 that our HST/ACS CMD has revealed the principal sequences of NGC 5466 with significantly higher precision than previous observations.

NGC 6779: Hatzidimitriou et al. (2004) and Rosenberg et al. (2000b) have both published CCD-based CMDs for this cluster that reach past the main sequence turnoff. The blue HB and relatively metal-poor nature of the cluster were noted by both studies. Additionally, our CMD exhibits a population of blue straggler stars as well as a better defined MSTO and unevolved MS suitable for age determination.

NGC 5053: Structurally similar to NGC 5466 discussed above, this cluster also presents an

<sup>&</sup>lt;sup>2</sup>Electronic versions of the photometry tables and fiducial sequences are available at http://www.astro.ufl.edu/~ata/GC\_Treasury/Web\_Page/.

exceptionally low stellar density, which is probably the main reason it has not been previously observed by *HST*. In addition, it also harbors a healthy population of blue straggler stars making it the focus of numerous stellar brightness variability studies. Color-magnitude diagrams have been presented by Rosenberg et al. (2000b), Sarajedini & Milone (1995), and Fahlman, Richer, & Nemec (1991), among others.

NGC~6144: The sole published CMD of this cluster is by Neely, Sarajedini, & Martins (2000); their BVI photometry reveals a cluster with a predominantly blue HB and significant differential reddening across its angular extent. This is because NGC 6144 is viewed behind the  $\rho$  Ophiuchi dust cloud approximately 40 arcmin northeast of the globular cluster NGC 6121 (M 4).

Palomar 2: Located in a direction of extremely high foreground absorption and differential reddening toward the Galactic anti-center, the CMD of this cluster presented by Harris et al. (1997) exhibits a significant amount of scatter. Nonetheless, these authors were able to characterize the HB morphology of Pal 2 as being bi-modal in color similar to that of NGC 1851, NGC 6229, and NGC 1261. As a result, they suggest that Pal 2 has a metallicity in the range  $[Fe/H]\sim-1.3\pm0.2$ . The features seen by Harris et al. (1997) are also present in Fig. 5 with the exception of a second MSTO feature blueward of the dominant MS at  $F606W \sim 23.5$  and  $(F606W - F814W) \sim 1.4$ . We return to an analysis of this feature and the metallicity of Pal 2 in Sec. 4.2. We note in passing that Pal 2 has gained renewed prominence recently because of a suggestion by Majewski et al. (2004) that it could be associated with the Sagittarius dwarf spheroidal galaxy.

E 3: The first CMD of this cluster was presented by van den Bergh, Demers, & Kunkel (1980) and later improved upon by McClure et al. (1985). Both of these studies noted two intriguing characteristics of this cluster. First, the equal-mass binary sequence in E 3 was among the most prominent ever observed to-date among globular clusters. Second, the cluster shows little or no indication of an HB population. Taken together, along with the dramatic decrease in stellar density along the lower MS, these findings suggest the presence of significant mass segregation and/or mass loss in E 3. Furthermore, these characteristics are consistent with the Galactic GC Pal 13 which Siegel et al. (2001) argue is in the last stages of being destroyed. The fact that E 3 does not possess a clear HB makes its distance and age determinations necessarily more uncertain. The most recent CMD by Rosenberg et al. (2000a) corroborates these results.

Lyngå 7: Thought to be an open cluster originally, Lyngå 7 was studied photometrically by Ortolani, Bica, & Barbuy (1993), who showed that it is more likely to be a (thick) disk globular cluster. Their CMD is heavily contaminated by non-cluster stars, but does reveal a prominent core-helium burning red clump and a putative main sequence turnoff that

suggested an age significantly younger than other Galactic globular clusters at its metallicity. However, a reanalysis of the Ortolani et al. (1993) CMD by Sarajedini (2004) indicates an age close to that of 47 Tuc. Our CMD is also heavily contaminated by non-cluster stars, but in the next section, we present a radially limited CMD which shows the cluster sequences better.

Palomar 1: First photometered by Ortolani & Rosino (1985) and later by Borissova & Spassova (1995), Pal 1 is similar to other low-density globular clusters such as Pal 13 and E 3 in that it exhibits an RGB and HB that are both very poorly populated. The more recent work of Rosenberg et al. (1998a; 1998b) has revealed a metallicity comparable with that of 47 Tuc, but an age that is some 4 to 5 Gyr younger than 47 Tuc. The possibility that Pal 1 has been misclassified as a globular cluster cannot be ruled out. In fact, Crane et al. (2003) have shown that Pal 1 could be a member of the Monoceros stream which has both open, transitional, and globular clusters as members (Frinchaboy et al. 2004), which is very interesting considering the ambiguity of Pal 1's classification.

NGC 6366: From the earliest CMD of this cluster by Pike (1976) to the most recent by Alonso et al. (1997) and Rosenberg et al. (2000b), it has been recognized that NGC 6366 is a close twin of 47 Tuc. Both clusters have predominantly red HBs, a metal abundance close to  $[Fe/H] \sim -0.7$  and a sparse RR Lyrae population, and, in fact, NGC 6366 is somewhat closer to us than 47 Tuc. The main reason NGC 6366 has received much less attention than 47 Tuc is because of its high extinction and significant differential reddening.

It is clear from the above discussion that many of the CMD features of these clusters have already been revealed by ground-based observations, especially those at magnitude levels above the MSTO. What makes the HST CMDs in Figs. 1 through 9 unique is that they represent the deepest photometry for these clusters published to-date. Most extend as much as seven magnitudes below the MSTO, in some cases, revealing a sequence of unresolved binaries that has never before been identified in these clusters. The binary populations of our target clusters will be discussed in a future paper. The HST CMDs presented herein are ideal for the determination of main sequence fitting distances, which is the subject of the next section, and ages, which are covered in Sec. 5.

## 4. Main Sequence Fitting

To minimize systematic errors associated with our filter set, we have chosen to perform main sequence fitting (MSF) in the ACS F606W and F814W filters. We have selected

three 'standard' clusters from our Treasury database - M92, NGC 6752, and 47 Tuc - as comparison clusters. Our fiducial sequences for M92 and NGC 6752 are consistent with those presented by Brown et al. (2005) and with the ground-based data of Stetson (2000) in the VI passbands. However, the Brown et al. (2005) fiducial for 47 Tuc is significantly bluer ( $\sim$ 0.04 mag) than our Treasury data and the photometry of Stetson (2000). We will address these issues more fully in a future paper, but, for the moment, it is important to point out that the MSF performed herein makes use of photometry for the target and comparison clusters that is internally consistent.

# 4.1. Cluster Properties

Table 2 lists the properties of the target and comparison clusters in the present study. The metallicities on the Zinn & West (1984) and Carretta & Gratton (1997) scales are taken from a number of sources. For NGC 5466, 5053, 6366, 6752, M 92, and 47 Tuc, both [Fe/H]<sub>ZW</sub> and [Fe/H]<sub>CG</sub> come from the globular cluster age-dating study of De Angeli et al. (2005), while for Pal 1, these values are measured by Rosenberg (1998b). The ZW and CG metallicities of NGC 6779 are derived by Hatzidimitriou et al. (2004) as part of their BVRI photometric study. For NGC 6144, Lyngå 7, and E 3, the ZW values come from Neely et al. (2000), Tavarez & Friel (1995), and Harris (1996), respectively, while the CG metallicities are calculated using the equation in Sec. 2.1 of De Angeli et al. (2005). The metallicity of Pal 2 is derived below in Sec. 4.2.

Columns 4 and 5 of Table 2 give the reddening and absolute distance modulus of each cluster from the Harris (1996) catalog. These have generally been calculated assuming  $M_v(HB) = 0.15$  [Fe/H] + 0.80 along with the mean apparent magnitude of the HB. This means that in cases where no HB is apparent (e.g. Pal 1, E 3) or differential reddening makes the level of the HB difficult to assess (Pal 2), the distances could be highly uncertain. Columns 6 and 7 are the reddenings and distance moduli derived via MSF in this paper. In the case of the comparison clusters, these values are taken from the study of Carretta et al. (2000), wherein globular cluster fiducials are fit to local subdwarfs with HIPPARCOS parallaxes.

The MS fits of the comparison cluster fiducials to the cluster CMDs are shown in Figs. 10 through 17. For NGC 6144, because its metal abundance lies between those of two standard clusters (M 92 and NGC 6752), we have fit both fiducials to NGC 6144 and interpolated the results. In performing the MS fits, we have shifted the fiducials of the comparison clusters in magnitude and color to match the unevolved MS of the target clusters. In particular, we match the data and the fiducial at a point ~2 magnitudes below the MSTO

of an old population which occurs at  $M_{\rm F606W} \sim +4.0$ . The shifts are then converted to reddenings and distance moduli using the color excess and absorption equations for a G2 type star given by Sirianni et al. (2005), namely E(F606W - F814W) = 0.98E(B - V) and  $A_{\rm F606W} = 2.85E(F606W - F814W)$ . The resultant reddenings and distance moduli were derived differentially from those of the comparison clusters. We estimate 1- $\sigma$  random errors of  $\pm 0.01$  mag and  $\pm 0.05$  mag, respectively, in the E(B - V) and  $(m - M)_0$  values.

It is instructive to consider our distance modulus results in light of the Harris (1996) values. Excluding E 3 and Pal 1, the values in Table 2 reveal a mean difference of  $\langle \Delta(m-M)_0 \rangle = 0.07 \pm 0.05$  between our distance moduli and those of Harris (1996) in the sense (Us–Harris). This is not surprising given that the MSF distances of our comparison clusters show a mean difference in the same sense of  $\langle \Delta(m-M)_0 \rangle = 0.15 \pm 0.02$  relative to the Harris (1996) values. Here and below, we use the small sample statistical formulae of Keeping (1962) to calculate the standard error of the mean.

Returning to E 3 and Pal 1, neither of these clusters exhibits a significant HB population in its CMD making the determination of distance especially challenging. The origin of the Harris (1996) distance for E 3 is quoted as the McClure et al. (1985) work. However, that paper makes no mention of a distance modulus for E 3, so it is not immediately clear what this distance is based on. As a result, it is difficult for us to reconcile the rather large difference of  $\Delta(m-M)_0=1.35$  mag between our distance modulus and that of Harris (1996) for E 3. In the case of Pal 1, the Harris (1996) values are taken from Rosenberg et al. (1998a) who used MSF to 47 Tuc to estimate Pal 1's distance. The precise value of the Pal 1 distance modulus from Rosenberg et al. (1998a) is given as  $(m-M)_0=15.25\pm0.25$ ; adopting a total error of  $\pm0.1$  mag for our distance modulus determination ( $\sigma_{\rm random} \sim 0.05$  mag and  $\sigma_{\rm systematic} \sim 0.10$  mag added in quadrature) leads to a difference of  $\Delta(m-M)_0=0.51\pm0.27$  in the sense (Us – Rosenberg), which is not statistically significant.

Turning now to a discussion of our derived reddenings, the mean difference between us and Harris is  $\langle \Delta E(B-V) \rangle = 0.044 \pm 0.013$  in the sense (Us–Harris). This excludes Pal 2, which has a very high and uncertain value. In contrast, this difference turns out to be  $\langle \Delta E(B-V) \rangle = 0.015 \pm 0.007$  for the comparison clusters. Based on this, one might argue that our derived reddening values are systematically too high. However, a different picture emerges when we compare to the reddening maps of Schlegel, Finkbeiner, & Davis (1998). Here we find a mean difference of  $\langle \Delta E(B-V) \rangle = -0.010 \pm 0.029$  for the target clusters and  $\langle \Delta E(B-V) \rangle = -0.015 \pm 0.014$  for the comparison clusters suggesting agreement with the Schlegel et al. maps. Note that we have excluded Pal 2 as above from this calculation and NGC 6144 which is located behind the  $\rho$  Ophiuchi dust cloud. We note in passing that the Schlegel et al. (1998) maps yield a reddening of E(B-V) = 0.91 for NGC 6144.

In addition to the distances and reddenings that are derived from the MSF procedure, we can also comment on the ages of the target clusters relative to the comparison clusters, which have similar metallicities. In particular, of the 9 clusters of interest (the case of Pal 2 is addressed in the next subsection), only Pal 1 appears to be significantly younger than its comparison cluster. There is also some indication that E 3 could be younger than 47 Tuc. While earlier work showed that Pal 1 is a relatively young cluster, there is no such expectation for E 3, as McClure et al. (1985) actually quote an age of 18 Gyr for this cluster. However, a more definitive statement about the age of E 3 will have to wait for a reliable abundance determination for this cluster. Previous papers on Lyngå 7 (Ortolani et al. 1993; Sarajedini 2004) suggested that it may be younger than 47 Tuc by as much as  $\sim 4$  Gyr. In contrast, our CMD unequivocally shows that the two are about the same age. We will return to the subject of cluster ages in Sec. 5. We should note as well that Pal 1 and E 3 show a strong depletion of low-mass stars. Even without quantitative luminosity functions, their CMDs show a striking decline of star numbers along the lower main sequence. To fully address this question will require, among other things, a more complete understanding of the photometric completeness of our data. We will address this phenomenon in a future paper.

## 4.2. The Special Case of Pal 2

Of the clusters in this study, Pal 2 is the most problematical in terms of applying the MSF technique. The CMD in Fig. 5 presents a main sequence that is so broadened by differential reddening that MSF seems intractable. However, there is an intriguing extension of the MS blueward and brightward of the MSTO / SGB region, as shown in the left panel of Fig. 18. Taking a cue from the photometric study of this cluster by Harris et al. (1997), we hypothesize that this feature represents a minimally reddened population in Pal 2 and proceed to investigate the spatial distribution of these stars. The filled circles in the right panel of Fig. 18 are the stars within the bounded region indicated in the left panel. The appearance of this figure suggests the presence of a region of minimal reddening in the southeast quadrant of the cluster. The concentric circles represent zones approximately centered on this region of Pal 2 for which CMDs are plotted in Fig. 19. The exact center of these circles has been chosen to yield a CMD in the innermost zone that best defines the cluster's principal sequences. The solid line in Fig. 19 is the fiducial sequence of NGC 6752 (Brown et al. 2005) shifted to match the main sequence of Pal 2 inside of 25" from the center. The reddening and distance of Pal 2 listed in Table 2 are derived from these shifts relative to NGC 6752. We estimate an error of  $\pm 0.05$  in E(B-V) and  $\pm 0.10$  mag in distance modulus.

Figure 19 corroborates our earlier hypothesis that the stars bounded by the region in the

left panel of Fig. 18 represent a population that is minimally reddened. As we move further from the southeast quadrant of the cluster, the reddening and its range increase so that the cluster sequences are redder and show greater scatter. In light of this apparent trend in the differential reddening, we have attempted to correct for its effects in the following manner. The first step involves the construction of a fiducial sequence for the cluster. Then each individual star yields a color residual, taken along the reddening direction in the CMD. From these residuals a reddening map is made, by finding the median residual in each 256x256-pixel square of the image. Then each star is corrected, along its reddening line, by an amount that is interpolated from the 16x16 points of the reddening map.

The result of this procedure is shown in Fig. 20 along with the fiducial sequence of NGC 6752 shifted along the reddening vector to match the principal sequence of Pal 2. The CMD of Pal 2 has tightened-up considerably better-defining the HB and the so-called 'RGB bump' that results from a pause in the brightward evolution of RGB stars (Fusi Pecci et al. 1990; Sarajedini & Forrester 1995; Ferraro et al. 1999).

The luminosity of the RGB Bump depends on the cluster metallicity and, to a lesser degree, the cluster age (Alves & Sarajedini 1999). As such, given that Pal 2 is likely to be an old cluster, we can use the magnitude difference between its HB and RGB Bump to estimate its metal abundance. The bottom panel of Fig. 20 illustrates the luminosity functions (LFs) of the RGB [1.7<(F606W-F814W)<2.3, filled circles] and HB [1.3<(F606W-F814W)<1.7, open circles], while the solid and dashed lines are the Gaussian fits to these distributions over the range 20.0 < F606W < 21.6. These fits yield a difference between the HB and Bump magnitudes of  $\Delta F606W_{\rm HB}^{\rm Bump} = -0.30 \pm 0.02$ . The error has been calculated by the adding the standard errors of the mean HB and Bump magnitudes in quadrature. Assuming that  $\Delta F606W_{\rm HB}^{\rm Bump} \approx \Delta V_{\rm HB}^{\rm Bump}$ , the relations given in Table 6 of Ferraro et al. (1999) give metallicities of [Fe/H]<sub>ZW</sub> =  $-1.68 \pm 0.04$  and [Fe/H]<sub>CG</sub> =  $-1.42 \pm 0.04$ . The quote errors on these quantities represent only the random errors. Thus, the metal abundance of Pal 2 is close to that of NGC 6752. In addition, the close match between the fiducial of NGC 6752 and the Pal 2 CMD suggests that the two clusters have comparable ages and metallicities.

#### 5. Isochrone Comparisons

#### 5.1. Construction of Theoretical Isochrones

Isochrones were generated from stellar evolution tracks produced by the Dartmouth Stellar Evolution Program (DSEP). DSEP employs high temperature opacities from OPAL (Iglesias & Rogers 1996), low temperature opacities from Ferguson et al. (2005), the detailed

equation of state code FreeEOS (Irwin 2004) for low mass stars, and surface boundary conditions derived from PHOENIX model atmospheres (Hauschildt et al. 1999a;1999b). The physical inputs (e.g. opacities, equation of state and convection theory) used in the stellar interior models are consistent with the physics used in the model atmosphere calculations. A detailed discussion of these new stellar models, color-Teff relations and isochrones is presented in Dotter et al. (2007, in preparation).

A grid of stellar evolution tracks were computed for [Fe/H]= -2.5, -2.0, -1.5, -1.0, -0.5, and 0.0 with  $[\alpha/\text{Fe}] = -0.2$ , 0.0, 0.2, 0.4, 0.6, and 0.8. Opacities and surface boundary conditions were created for each specific composition listed. Stellar masses between 0.1 and 1.5  $\mathcal{M}_{\odot}$  allow for isochrones with ages ranging from 3 to 15 Gyr that extend from  $M_V \sim 14$  to the tip of the RGB.

For comparison purposes, the isochrones were transformed using two different color- $T_{\rm eff}$  relations. Both transformations include standard ground-based B, V, and I magnitudes along with HST filters F606W and F814W (both ACS-WFC and WFPC2). The semi-empirical transformation uses the B, V, and I magnitudes from VandenBerg & Clem (2003) and the relevant equations to convert from V and I to F606W and F814W in Appendix D of Sirianni et al. (2005). The synthetic color- $T_{\rm eff}$  transformation uses fluxes from the PHOENIX model atmospheres (also used for surface boundary conditions) along with the definitions of B, V, and I from Bessell (1990) and HST ACS/WFC and WFPC2 filters from Sirianni et al. (2005), all normalized to the Vega system. The semi-empirical color transformation has the advantage of being constrained to fit observational data from globular clusters at low metallicities but does not explicitly account for the effects of  $\alpha$ -enhancement. The synthetic color transformation, on the other hand, accounts for the influence of  $\alpha$ -enhancement but suffers from poor fits to the MSTO and subgiant regions that are typical of theoretical color transformations.

# 5.2. Comparison to Cluster CMDs

Given that the ZW and CG metallicities usually differ by less than  $\sim 0.2$  dex, we adopt the latter abundance values in the isochrone fits. To select the appropriate ratio of the  $\alpha$ -elements to iron, we assume that  $[\alpha/\text{Fe}] = +0.4$  for [Fe/H] < -1.0 and  $[\alpha/\text{Fe}] = +0.2$  for  $[\text{Fe/H}] \sim -0.7$ . These  $[\alpha/\text{Fe}]$  values reflect the general trend observed in thick disk and halo stars (e.g. Origlia & Rich 2004; Boesgaard et al. 2005; Meléndez et al. 2006; Reddy et al. 2006). We use the MSF distance and reddening in Table 2 as a starting point; then we vary the distance and reddening until a satisfactory correspondence is achieved between the MS of the cluster and the isochrone making sure that the point  $\sim 2$  magnitudes below an old

MSTO (i.e.  $M_{\rm F606W} \sim +6.0$ ) matches, similar to the MSF technique performed earlier. The results are shown in Figs. 21 through 28. Pal 2 is excluded because the MS is not adequately defined to allow a comparison of the isochrone to the cluster's unevolved MS. However, as noted above, its age is likely to be close to that of NGC 6752.

Examination of the isochrone fits reveals the following. The fit to the unevolved MS stars is relatively good for the metal-poor clusters and degrades for the empirical color-Teff transformation as metallicity increases. In this case, the models tend to be redder than the observational data. In contrast, the synthetic transformation provides a better correspondence with the photometry of the MS. The poor match to the lower main sequence could be due to either difficulities with the effective temperatures predicted by the models, or with the color-temperature relations. We are currently investigating this issue.

As expected from the MSF results, the isochrone fits of NGC 5466, 6779, 5053, 6144, Lyngå 7, and NGC 6366 reveal ages in the range of 12 to 14 Gyr. In contrast, the age of E 3 appears to be about 2 Gyr younger than these clusters while the age of Pal 1 could be as much as 8 Gyr younger. The typical error on these ages is between 1 and 2 Gyr primarily because they depend on the uncertain distances and reddenings of the clusters. In a future paper, we will address the issues of relative and absolute GC ages using more robust techniques. We emphasize that, as noted in Sec. 4, the age of E 3 is likely to be especially uncertain until a more reliable metallicity is determined for it.

#### 6. Summary and Conclusions

We have presented the first HST-based CMDs for the Galactic globular clusters NGC 5446, 6779, 5053, 6144, Pal 2, E 3, Lyngå 7, Pal 1, and NGC 6366. The CMDs extend reliably from the horizontal branch to as much as seven magnitudes fainter than the main sequence turnoff. Features revealed in these diagrams include the HB morphology, the presence of blue straggler stars, unresolved-binary populations parallel to the main sequence, and possibly white dwarf populations.

Using fiducial sequences for three standard clusters (M 92, NGC 6752, and 47 Tuc) with well-known metallicities and distance moduli, we perform main sequence fitting on the target clusters in order to obtain estimates of their distances and reddenings. These comparisons along with fitting the cluster main sequences to theoretical isochrones provide estimates of the clusters' ages. We find that only E3 and Pal 1 are significantly younger than the standard cluster to which they are compared. E3 is  $\sim$ 2 Gyr younger than 47 Tuc and Pal 1 could be as much as 8 Gyr younger than 47 Tuc. The ages of the remaining clusters are consistent

with the standard clusters at their metallicities.

Support for this work (proposal number GO-10775) was provided by NASA through a grant from the Space Telescope Science Institute which is operated by the Association of Universities for Research in Astronomy, Incorporated, under NASA contract NAS5-26555.

#### REFERENCES

- Alonso, A., Salaris, M., Martinez-Roger, C., Straniero, O., & Arribas, S. 1997, A&A, 323, 374
- Alves, D., & Sarajedini, A. 1999, ApJ, 511, 225
- Anderson, J. 2006, 2005 HST Calibration Workshop Proceedings, Koekemoer, A., Goufrooij, P., & Dressel, eds
- Anderson, J. & King, I. 2006, ACS/ISR 2006-01
- Bedin, L., Cassisi, S., Castelli, F., Piotto, G., Anderson, J., Salaris, M., Momany, Y., & Pietrinferni, A. 2005, MNRAS, 357, 1038
- Bessell, M. S. 1990, PASP, 102, 1181
- Boesgaard, A.M., King, J.R., Cody, A.M., Stephens, A., & Deliyannis, C.P. 2005, ApJ, 629, 832
- Borissova, J., & Spassova, N. 1995, A&AS, 110, 1
- Brown, T. M., Ferguson, H. C., Smith, E., Guhathakurta, P., Kimble, R. A., Sweigart, A. V., Renzini, A., Rich, R. M., & VandenBerg, D. A. 2005, AJ, 130, 1693
- Carretta, E., & Gratton, R. G. 1997, A&AS, 121, 95
- Carretta, E., Gratton, R. G., Clementini, G., & Fusi Pecci, F. 2000, ApJ, 533, 215
- Chaboyer, B., Fenton, W. H., Nelan, J. E., Patnaude, D. J., & Simon, F. 2001 ApJ, 562, 521
- Corwin, T. M., Carney, B. W., & Nifong, B. G. 1999, AJ, 118, 2875
- Crane, J. D., Majewski, S. R., Rocha-Pinto, H. J., Frinchaboy, P. M., Skrutskie, M. F., & Law, D. R. 2003, ApJ, 594, L119

- De Angeli, F., Piotto, G., Cassisi, S., Busso, G., Recio-Blanco, A., Salaris, M., Aparicio, A., & Rosenberg, A., 2005, AJ, 130, 116
- Fahlman, G. G., Richer, H. B., & Nemec, J. 1991, ApJ, 380, 124
- Ferguson, J. W., Alexander, D. R., Allard, F., Barman, T., Bodnarik, J. G., Hauschildt, P. H., Heffner-Wong, A., & Tamanai, A. 2005, ApJ, 623, 585
- Ferraro, F. R., Messineo, M., Fusi Pecci, F., de Palo, M. A., Straniero, O., Chieffi, A., & Limongi, M. 1999, AJ, 118, 1738
- Frinchaboy, P. M., Majewski, S. R., Crane, J. D., Reid, I. N., Rocha-Pinto, H. J., Phelps, R. L., Patterson, R. J., & Muñoz, R. R. 2004, ApJ, 602, L21
- Fusi Pecci, F., Ferraro, F. R., Crocker, D. A., Rood, R. T., & Buonanno, R., 1990, A&A, 238, 95
- Harris, W. E. 1996, AJ, 112, 1487
- Harris, W. E., Durrell, P. R., Petitpas, G. R., Webb, T. M., & Woodworth, S. C. 1997, AJ, 114, 1043
- Hatzidimitriou, D., Antoniou, V., Papadakis, I., Kaltsa, M., Papadaki, C., Papamastorakis, I., & Croke, B. F. W. 2004, MNRAS, 348, 1157
- Hauschildt, P. H., Allard, F. & Baron, E. 1999a, ApJ, 512, 377
- Hauschildt, P., H., Allard, F., Ferguson, J., Baron, E., & Alexander, D. 1999b, ApJ, 525, 871
- Iglesias, C. A. & Rogers, F. J. 1996, ApJ, 464, 943
- Irwin, A. 2004, Technical Report (http://freeeos.sourceforge.net)
- Jeon, Y.-B., Lee, M. G., Kim, S.-L., & Lee, H. 2004, AJ, 128, 287
- Keeping, E. S. 1962, Introduction to Statistical Inference (Van Nostrand, Princeton) p. 202
- Majewski, S. et al. 2004, AJ, 128, 245
- Meléndez, J., Shchukina, N. G., Vasiljeva, I. E., & Ramírez, I. 2006, ApJ, 642, 1082
- McClure, R. D., Hesser, J. E., Stetson, P. B., & Stryker, L. L. 1985, PASP, 97, 665
- Neely, R. K., Sarajedini, A., & Martins, D. H. 2000, AJ, 119, 1793

Origlia, L., & Rich, R.M. 2004, AJ, 127, 3422

Ortolani, S., & Rosino, L. MmSAI, 50, 105

Ortolani, S., Bica, E., & Barbuy, B. 1993, A&A, 273, 415

Pike, C. D. 1976, MNRAS, 177, 257

Reddy, B.E., Lambert, D.L., & Allende Prieto, C. 2006, MNRAS, 367, 1329

Reiss, A., & Mack, J. 2004, ACS-ISR 04-06

Rosenberg, A., Saviane, I., Piotto, G., Aparicio, A., & Zaggia, S. R. 1998a, AJ, 115, 648

Rosenberg, A., Piotto, G., Saviane, I., Aparicio, A., & Gratton, R. 1998b, AJ, 115, 658

Rosenberg, A., Piotto, G., Saviane, I., & Aparicio, A. 2000a, A&AS,144, 5

Rosenberg, A., Aparicio, A., Saviane, I., & Piotto, G. 2000b, A&AS,145, 451

Sarajedini, A. 2004, AJ, 128, 1228

Sarajedini, A., & Forrester, W. 1995, AJ, 109, 1112

Sarajedini, A. & Milone, A. A. E. 1995, AJ, 109, 269

Schlegel, D. J., Finkbeiner, D. P., & Davis, M. 1998, ApJ, 500, 525

Siegel, M. H., Majewski, S. R., Cudworth, K. M., & Takamiya, M. 2001, AJ, 121, 935

Sirianni, M. et al. 2005, PASP, 117, 1049

Stetson, P. B. 1987, PASP, 99, 191

Stetson, P. B. 1994, PASP, 106, 250

Stetson, P. B. 2000, PASP, 112, 925

Tavarez, M., & Friel, E. 1995, AJ, 110, 223

van den Bergh, S., Demers, S., & Kunkel, W. E. 1980, ApJ, 239, 112

VandenBerg, D. A., & Clem, J. L. 2003, AJ,126, 778

Zinn, R. J., & West, M. J. 1984, ApJS, 55, 45

This preprint was prepared with the AAS IATEX macros v5.2.

Table 1. Observing Log

Cluster	α <sub>2000</sub> (h m s)	$\delta_{2000}$ (° ' ")	l (°)	ь (°)	Dataset	UT Date	Filter	Exp Time
NGC 5466	14 05 27.3	+28 32 04	42.15	73.59	J9L903	2006-04-12	F606W F814W	1 x 30s, 5 x 340s 1 x 30s, 5 x 350s
NGC 6779 (M56)	19 16 35.5	+30 11 05	62.66	8.34	J9L905	2006-05-11	F606W F814W	1 x 20s, 5 x 340s 1 x 20s, 5 x 350s
NGC 5053	13 16 27.0	+17 41 53	335.69	78.94	J9L902	2006-03-06	F606W F814W	1 x 30s, 5 x 340s 1 x 30s, 5 x 350s
NGC 6144	16 27 14.1	-26 01 29	351.93	15.70	J9L943	2006-04-15	F606W F814W	1 x 25s, 5 x 340s 1 x 25s, 5 x 350s
Palomar 2	04 46 05.9	+31 22 51	170.53	-9.07	J9L908	2006-08-08	F606W F814W	5 x 380s 5 x 380s
E 3	09 20 59.3	-77 16 57	292.27	-19.02	J9L906	2006-04-15	F606W F814W	1 x 5s, 4 x 100s 1 x 5s, 4 x 100s
Lyngå 7	16 11 03.0	-55 18 52	328.77	-2.79	J9L904	2006-04-07	F606W F814W	1 x 35s, 5 x 360s 1 x 35s, 5 x 360s
Palomar 1	03 33 23.0	+79 34 50	130.07	19.03	J9L901	2006-03-17	F606W F814W	1 x 15s, 5 x 390s 1 x 15s, 5 x 390s
NGC 6366	17 27 44.3	-05 04 36	18.41	16.04	J9L907	2006-03-30	F606W F814W	1 x 10s, 4 x 140s 1 x 10s, 4 x 140s

Table 2. Cluster Parameters

Cluster	$[Fe/H]_{\mathrm{ZW}}$	$[Fe/H]_{\mathrm{CG}}$	$E(B-V)^{a}$	$(m-M)_0^a$	$E(B-V)^{\mathrm{b}}$	$(m-M)_0^{\mathrm{b}}$				
			Target Clusters							
NGC 5466	-2.22	-2.20	0.00	16.00	0.02	16.03				
NGC 6779 (M 56)	-2.20	-2.00	0.20	15.03	0.26	15.08				
NGC 5053	-2.10	-1.98	0.04	16.07	0.01	16.22				
NGC 6144	-1.81	-1.56	0.36	14.64	0.45	14.61				
Palomar 2	-1.68	-1.42	1.24	17.21	0.94	17.13				
E 3	-0.80	-0.83	0.30	13.19	0.34	14.54				
Lyngå 7	-0.62	-0.64	0.73	14.28	0.78	14.55				
Palomar 1	-0.6	-0.7	0.15	15.19	0.23	15.76				
NGC 6366	-0.58	-0.73	0.71	12.77	0.75	12.87				
Comparison Clusters										
NGC 6341 (M 92)	-2.24	-2.16	0.02	14.58	0.025	14.66				
NGC 6752	-1.54	-1.24	0.04	13.01	0.035	13.23				
NGC 104 (47 Tuc)	-0.71	-0.78	0.04	13.25	0.055	13.40				

<sup>&</sup>lt;sup>a</sup>Data from Harris (1996). Absolute distance modulus has been computed assuming  $A_V=3.1E(B-V)$ .

<sup>&</sup>lt;sup>b</sup>Results from main sequence fitting.

- Fig. 1.— The color-magnitude diagram for NGC 5466 in the VEGAmag system. The plus symbols represent stars that are affected by at least one saturated pixel in either or both of the F606W and F814W images. This diagram contains 21,449 stars and extends to approximately 12% of the tidal radius of 34′ (Harris 1996).
- Fig. 2.— Same as Fig. 1 except that the CMD of NGC 6779 (M56) is shown containing 61,056 stars and extending to about 50% of the tidal radius of 8.5' (Harris 1996).
- Fig. 3.— Same as Fig. 1 except that the CMD of NGC 5053 is shown containing 15,618 stars and extending to about 30% of the tidal radius of 14′ (Harris 1996).
- Fig. 4.— Same as Fig. 1 except that the CMD of NGC 6144 is shown containing 19,442 stars and extending to about 13% of the tidal radius of 33′ (Harris 1996).
- Fig. 5.— Same as Fig. 1 except that the CMD of Palomar 2 is shown containing 43,242 stars and extending to about 60% of the tidal radius of 6.8' (Harris 1996). The arrow is the reddening vector for E(F606W F814W) = 0.3.
- Fig. 6.— Same as Fig. 1 except that the CMD of E3 is shown containing 852 stars and extending to about 40% of the tidal radius of 11′ (Harris 1996).
- Fig. 7.— Same as Fig. 1 except that the CMD of Lyngå7 is shown containing 32,226 stars. The tidal radius for Lyngå7 is not given in the Harris (1996) compilation. The arrow is the reddening vector for E(F606W F814W) = 0.3.
- Fig. 8.— Same as Fig. 1 except that the CMD of Palomar 1 is shown containing 808 stars and extending to about 47% of the tidal radius of 9.0′ (Harris 1996).
- Fig. 9.— Same as Fig. 1 except that the CMD of NGC 6366 is shown containing 5,503 stars and extending to about 27% of the tidal radius of 15′ (Harris 1996).
- Fig. 10.— The result of fitting the fiducial sequence of M92 to the main sequence of NGC 5466. The small open squares are M92 HB stars. The plus symbols represent stars that are affected by at least one saturated pixel in either or both of the F606W and F814W images.

- Fig. 11.— Same as Fig. 10 except that the CMD of NGC 6779 (M56) is shown.
- Fig. 12.— Same as Fig. 10 except that the CMD of NGC 5053 is shown.
- Fig. 13.— The result of fitting the fiducial sequences of M92 (left panel) and NGC 6752 (right panel) to the main sequence of NGC 6144. The small open squares are the HB stars of M92 (left) and NGC 6752 (right). The plus symbols represent stars that are affected by at least one saturated pixel in either or both of the F606W and F814W images.
- Fig. 14.— The result of fitting our fiducial sequence of 47 Tuc to the main sequence of E3. The small open squares the HB stars in 47 Tuc. The plus symbols represent stars that are affected by at least one saturated pixel in either or both of the F606W and F814W images.
- Fig. 15.— Same as Fig. 14 except that the CMD of Lyngå7 is shown for stars less than 15" from the cluster center.
- Fig. 16.— Same as Fig. 14 except that the CMD of Pal 1 is shown.
- Fig. 17.— Same as Fig. 14 except that the CMD of NGC 6366 is shown.
- Fig. 18.— The left panel shows the CMD of Pal 2 with the main sequence 'extension' indicated by a box-like region. The right panel shows the location of stars (filled circles) in this box relative to other stars in the cluster field. The circles are drawn at radii of 25", 50", 100", and 150" and centered at (1800,2400) pixels.
- Fig. 19.— The radial CMDs of Pal 2 centered on (1800,2400) pixels (see Fig. 11). The fiducial and HB stars are those of NGC 6752 shifted to the distance and reddening of the data in the inner region (upper left panel).
- Fig. 20.— The upper panel shows the differential-reddening-corrected CMD for Pal 2 along with the fiducial sequence of NGC 6752 shifted along the reddening vector to match the principal sequences of Pal 2. The lower panel displays the RGB (filled circles) and HB (open circles) LFs of Pal 2 along with the corresponding Gaussian fits (solid and dashed lines).
- Fig. 21.— The CMD of NGC 5466 along with theoretical isochrones based on two different color- $T_{\rm eff}$  transformations (see text).
- Fig. 22.— Same as Fig. 21 except that the CMD of NGC 6779 (M56) is plotted.

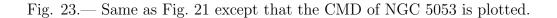


Fig. 24.— Same as Fig. 21 except that the CMD of NGC 6144 is plotted.

Fig. 25.— Same as Fig. 21 except that the CMD of E3 is plotted.

Fig. 26.— Same as Fig. 21 except that the CMD of Lyngå7 is plotted for stars inside of 15" from the cluster center.

Fig. 27.— Same as Fig. 21 except that the CMD of Palomar 1 is plotted.

Fig. 28.— Same as Fig. 21 except that the CMD of NGC 6366 is plotted.

This figure "f1.jpg" is available in "jpg" format from:

This figure "f2.jpg" is available in "jpg" format from:

This figure "f3.jpg" is available in "jpg" format from:

This figure "f4.jpg" is available in "jpg" format from:

This figure "f5.jpg" is available in "jpg" format from:

This figure "f6.jpg" is available in "jpg" format from:

This figure "f7.jpg" is available in "jpg" format from:

This figure "f8.jpg" is available in "jpg" format from:

This figure "f9.jpg" is available in "jpg" format from:

This figure "f10.jpg" is available in "jpg" format from:

This figure "f11.jpg" is available in "jpg" format from:

This figure "f12.jpg" is available in "jpg" format from:

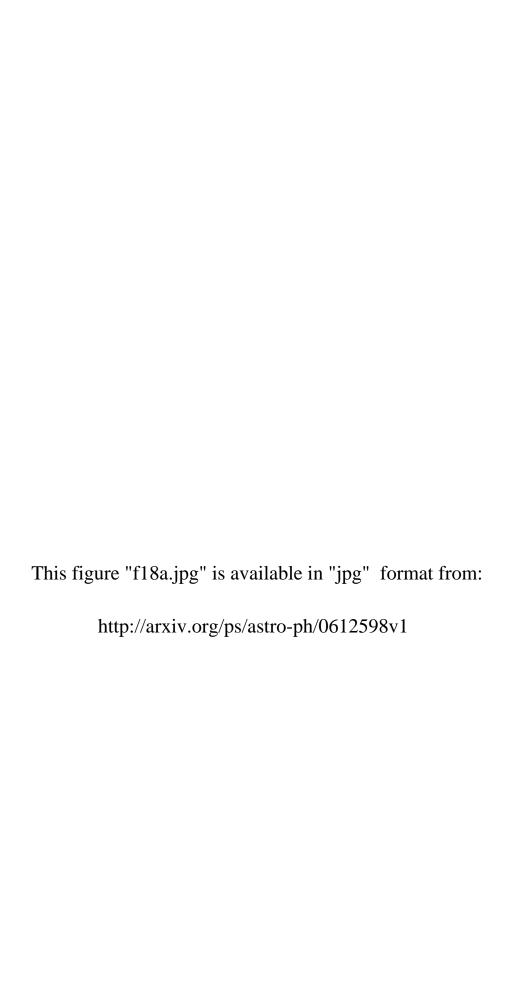
This figure "f13.jpg" is available in "jpg" format from:

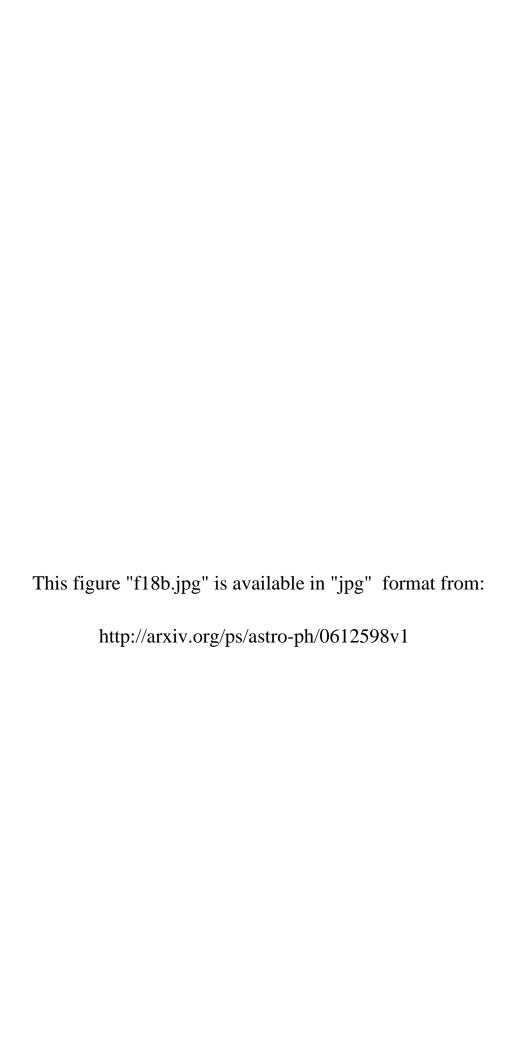
This figure "f14.jpg" is available in "jpg" format from:

This figure "f15.jpg" is available in "jpg" format from:

This figure "f16.jpg" is available in "jpg" format from:

This figure "f17.jpg" is available in "jpg" format from:





This figure "f19.jpg" is available in "jpg" format from:

This figure "f20.jpg" is available in "jpg" format from:

This figure "f21.jpg" is available in "jpg" format from:

This figure "f22.jpg" is available in "jpg" format from:

This figure "f23.jpg" is available in "jpg" format from:

This figure "f24.jpg" is available in "jpg" format from:

This figure "f25.jpg" is available in "jpg" format from:

This figure "f26.jpg" is available in "jpg" format from:

This figure "f27.jpg" is available in "jpg" format from:

This figure "f28.jpg" is available in "jpg" format from: